AD-A134 041 THEORETICAL MODELING OF THE PLASMA EROSION OPENING SWITCH FOR INDUCTIVE STORAGE APPLICATIONS(U) NAVAL RESEARCH LAB WASHINGTON DC P F OTTINGER ET AL. 1/1

UNCLASSIFIED 27 OCT 83 NRL-MR-5205 F/G 9/1 NL

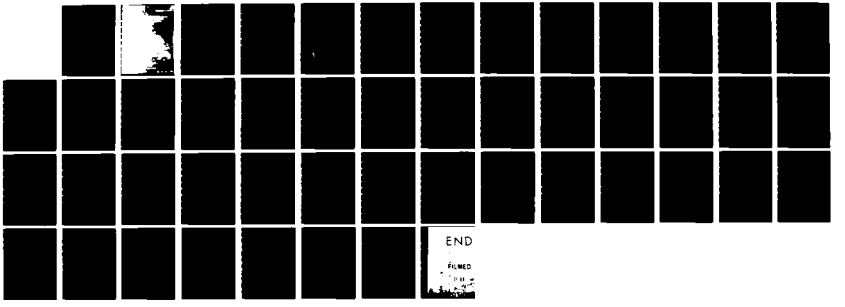

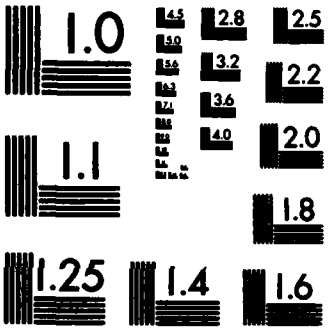

SECURITY CLASSIFICATION OF THIS PAGE (When Data Entered)

REPORT DOCUMENTATION PAGE		READ INSTRUCTIONS BEFORE COMPLETING FORM
1. REPORT NUMBER NRL Memorandum Report 5205	2. GOVT ACCESSION NO.	3. RECIPIENT'S CATALOG NUMBER
4. TITLE (and Subtitle) THEORETICAL MODELING OF THE PLASMA EROSION OPENING SWITCH FOR INDUCTIVE STORAGE APPLICATIONS		5. TYPE OF REPORT & PERIOD COVERED Interim report on a continuing NRL problem. 6. PERFORMING ORG. REPORT NUMBER
7. AUTHOR(s) P.F. Ottinger,* Shyke A. Goldstein,* and R.A. Meger		8. CONTRACT OR GRANT NUMBER(s)
9. PERFORMING ORGANIZATION NAME AND ADDRESS Naval Research Laboratory Washington, DC 20375		10. PROGRAM ELEMENT, PROJECT, TASK AREA & WORK UNIT NUMBERS DE-AI08-79DP40092; 47-0879-0-3; 47-0875-0-3
11. CONTROLLING OFFICE NAME AND ADDRESS Department of Energy Washington, DC 20545 Defense Nuclear Agency Washington, DC 20305		12. REPORT DATE October 27, 1983 13. NUMBER OF PAGES 46
14. MONITORING AGENCY NAME & ADDRESS(if different from Controlling Office)		15. SECURITY CLASS. (of this report) UNCLASSIFIED 15a. DECLASSIFICATION/DOWNGRADING SCHEDULE

16. DISTRIBUTION STATEMENT (of this Report)

Approved for public release; distribution unlimited.

17. DISTRIBUTION STATEMENT (of the abstract entered in Block 20, if different from Report)

18. SUPPLEMENTARY NOTES

*Present address: JAYCOR, Inc., Alexandria, VA 22304

This work was supported in part by the U.S. Department of Energy and the Defense Nuclear Agency under Subtask T99QAXLA, work unit 00038, and work unit title "Advanced Beam Generation Concepts."

19. KEY WORDS (Continue on reverse side if necessary and identify by block number)

Plasma erosion opening switch (PEOS)	Inductive storage system
Switch model	Load current
Circuit analysis	Output pulse
Transmission line code	Power multiplication

20. ABSTRACT (Continue on reverse side if necessary and identify by block number)

A theoretical model for the plasma erosion opening switch (PEOS) is presented which predicts its voltage, current and impedance history as a function of the input waveforms, geometry and switch parameters. Scaling laws for the switch operation are developed from this model. System requirements for pulse compression and power multiplication using inductive storage are derived from a simple lumped circuit analysis and a transmission line analysis. These requirements are shown to be

(Continues)

DD FORM 1 JAN 73 1473 EDITION OF 1 NOV 65 IS OBSOLETE
S/N 0102-014-6601

SECURITY CLASSIFICATION OF THIS PAGE (When Data Entered)

20. ABSTRACT (Continued)

satisfied using the PEOS as a fast opening, vacuum switch in a configuration relevant for existing high power accelerators. The switch model is incorporated into a transmission line code for comparison with recent inductive storage experiments. Code results agree well with the data and show conduction times of ~ 60 ns, switching times of ~ 10 ns with peak currents of ~ 600 kA.

approx.

CONTENTS

THEORETICAL MODELING OF THE PLASMA EROSION OPENING SWITCH FOR INDUCTIVE STORAGE APPLICATIONS

I. Introduction

Recent experiments have demonstrated that the plasma erosion opening switch (PEOS) can be used as a fast opening vacuum output switch on existing pulsed power generators.[1] As much as ~600 kA of current has been conducted through the switch for up to 60 ns before being diverted to a load in less than 10 ns. Terrawatt-level pulsed power applications for such switches are manyfold including prepulse suppression,[2,3] risetime sharpening,[2,3] inductive storage and power multiplication through pulse compression.[1] Previous experiments were successful in suppressing prepulse with similar switches[2] and suggested the possibility of the present opening switch work for inductive storage applications.

Opening switch research for similar time scales is also being pursued using other techniques. These include among others the e-beam controlled switch,[4] the plasma flow switch,[5] dense plasma focus switch[6] and the reflex switch.[7] Each switch uses a different technique for rapidly increasing its impedance after carrying large currents for some conduction time. Each operates in a different current and voltage regime and has a conduction time ranging from tens of nanoseconds to hundreds of nanoseconds. Switching or opening times vary from nanoseconds to hundreds of nanoseconds. The PEOS is of particular interest because it is a vacuum switch which provides the appropriate conduction time (~100 ns) and opening time (~10 ns) at high power (~1 TW) for inductive storage applications using a state-of-the-art pulsed power generator as the current charging device.

Manuscript approved August 30, 1983.

System requirements for pulse compression and power multiplication using inductive storage techniques are outlined in Section II of this paper. A simple lumped circuit analysis is used to obtain these requirements and then transmission line effects are discussed. In Section III the model that is used to describe the operation of the PEOS is presented. Scaling laws for the switch are derived in Section IV and these are used to show that the PEOS satisfies the switch requirements found in Section II. Results from a transmission line code analysis incorporating the PEOS model are given in Section V and compared with experimental data in Section VI. A discussion of the results of this work is given in Section VII.

II. System Requirements

Assume that one would like to design an inductive storage system which will provide for pulse compression and power multiplication of the output pulse from a high power accelerator. For a given accelerator the storage inductance, load resistance and inductance, and opening switch characteristics should be chosen in order to maximize the energy transfer from the accelerator to the load while obtaining the desired pulse compression and power multiplication. Important switch characteristics include the switch opening time and the initial and final switch resistances. First a simple lumped circuit analysis is used to derive expressions for the relevent timescales, the peak load power and the energy transfer efficiency for such a system. Then a simple transmission line analysis is used to illustrate transit time effects which are not included in the lumped circuit analysis.

A. Lumped Circuit Analysis

System requirements for pulse compression and power multiplication using inductive storage techniques can be best understood by analyzing the simple lumped circuit shown in Fig. 1. At time t=0 it is assumed that the storage inductor L_1 is current charged to $I_1(0)=I_o$ by the generator whose open circuit voltage now drops to zero. In order to efficiently charge the inductor, L_1 is chosen so that $L_1/R_g \sim \tau_p$ where τ_p is the generator pulse duration and R_g represents the generator impedance. The switch impedance which until this time was assumed to be zero, now rises instantaneously to a value R_s. A small inductor, L_2, placed between the switch and the load resistance, R_ℓ, represents the finite inductance required for the feed between the switch and the load. Initially the current $I_2(0)=0$. The opening time of the switch, τ_{op}, which is defined to be the time for the switch impedance to rise from its initial small value to its final large value, has been assumed to be zero. The risetime of the load current, which will be called the switching time, τ_s, is not instantaneous and depends on the switch and load characteristics. In general τ_s is finite and $\tau_s > \tau_{op} \geq 0$. Thus energy will be lost to switch heating as current flows through the switch during the switching time. One objective for designing an optimum switching system is to minimize this energy loss.

When $t > 0$, the circuit equations for $I_1(t)$ and $I_2(t)$ are

$$0 = R_g I_1 + L_1 dI_1/dt + R_s(I_1 - I_2) , \tag{1}$$

$$0 = R_\ell I_2 + L_2 dI_2/dt + R_s(I_2 - I_1) . \tag{2}$$

For simplicity the open circuit voltage on the left hand side of Eq. (1) has been set to zero at the time the switch begins to open (i.e. at t=0). The

more general case with a nonzero value on the left hand side of Eq. (1) could be treated by the same techniques presented here. These two coupled equations can be solved simultaneously to yield the characteristic roots

$$\tau_{\pm}^{-1} = \left[\frac{R_\ell + R_s}{2L_2} + \frac{R_g + R_s}{2L_1}\right]\left[1 \pm \left(1 - \frac{4L_1L_2\left[(R_\ell+R_s)(R_g+R_s)-R_s^2\right]}{\left[L_1(R_\ell+R_s) + L_2(R_g+R_s)\right]^2}\right)^{1/2}\right] \tag{3}$$

This expression is simplified in the limits that R_s is much larger than R_ℓ or R_g and that L_1 is much larger than L_2. The first condition states that the switch opens to an impedance larger than the other impedances in the circuit and therefore allows the current to switch. The second condition follows from the requirements that the inductance L_1 is large for storing energy and L_2 is small so that the load current can rise rapidly. In these limits

$$\tau_+ = L_2/R_s \tag{4a}$$

$$\tau_- = L_1/(R_g + R_\ell) \ , \tag{4b}$$

with $\tau_+ \ll \tau_-$.

Using the initial conditions, $I_1(0)=I_o$ and $I_2(0)=0$, one finds that

$$I_1(t) \approx \frac{L_1 I_o}{(L_1+L_2)}\left[\exp(-t/\tau_-) + \frac{L_2}{L_1}\exp(-t/\tau_+)\right] \ , \tag{5}$$

$$I_2(t) \approx \frac{L_1 I_o}{(L_1+L_2)}\left[\exp(-t/\tau_-) - \exp(-t/\tau_+)\right] \ , \tag{6}$$

and that the switch current $I_s = I_1 - I_2$ is given by

$$I_s(t) \approx I_o \exp(-t/\tau_+) \ . \tag{7}$$

In this case the switching time $\tau_s = \tau_+$. Because $\tau_+ \ll \tau_-$, the pulse width of the

load current scales roughly as τ_-, so that the output pulse width is just the decay time of the storage inductor current through the load resistance and generator impedance. One sees that for a fast output risetime the choice of small L_2 and large R_s were appropriate. In addition, the ratio of the input pulse width τ_p to the output pulse width τ_- is $\tau_p/\tau_- \sim (R_g+R_\ell)/R_g$. Thus for larger R_ℓ the output pulse width is narrower, however, the narrowness of the output pulse width is limited by transmission line effects as discussed in Sec. II.B.

The power delivered to the load, $P = I_2^2 R_\ell$, has a peak value of

$$P_p \approx \frac{R_\ell L_1^2 I_o^2}{(L_1+L_2)^2}\left(1-\frac{2}{x}\left[\ell n(x)+1\right]\right) , \tag{8}$$

where

$$x = R_s L_1/[L_2(R_g+R_\ell)] >> 1. \tag{9}$$

This power level should be compared with the power the generator can deliver to a matched load ($R_\ell = R_g$, $L_1 = L_2 = 0$ and $R = \infty$) in order to assess the power multiplication. For a square wave voltage pulse the peak power into a matched load is $P_m = V_o^2/4R_g$, where V_o is the peak open circuit voltage. If this same square wave open circuit voltage of duration τ_p is applied across the circuit in Fig. 1 with $R_s = 0$, the current in the inductor is

$$I_o = \frac{V_o}{R_g}\left[1-\exp(-R_g\,\tau_p/L_1)\right] \tag{10}$$

The power multiplication factor, $M = P_p/P_m$, is then

$$M \approx \frac{4R_\ell}{R_g} \frac{L_1^2}{(L_1+L_2)^2} \left[1-\exp\left(-\frac{R_g \tau_p}{L_1}\right)\right]^2 \left(1-\frac{2}{x}\left[\ell n(x)+1\right]\right) \qquad (11)$$

The important scaling here is that M increases linearly with R_ℓ/R_g. Thus the load resistance should be large compared with the generator impedance in order to achieve high power multiplication.

The energy delivered to the load, E_ℓ, is just the integral of $I_2^2 R_\ell$ from t=0 to ∞. Using Eqs. (4), (6) and (10), one finds

$$E_\ell = \frac{L_1^3 V_o^2 R_\ell}{2R_g^2(R_g+R_\ell)(L_1+L_2)^2} \left[1-\exp(-R_g\tau_p/L_1)\right]^2 . \qquad (12)$$

Normalizing this to the energy delivered to a matched load, $E_m=V_o^2\tau_p/4R_g$, gives a measure of the energy transfer efficiency,

$$\frac{E_\ell}{E_m} = \left[\frac{R_\ell}{R_g+R_\ell}\right]\left[\frac{L_1^2}{(L_1+L_2)^2}\right]\left[\frac{2L_1}{\tau_p R_g}\left(1-\exp\left[-R_g\tau_p/L_1\right]\right)^2\right] . \qquad (13)$$

There are three sources of energy loss. First, energy is reflected back into the generator during the charging of the storage inductor. This can be associated with the last term in square brackets in Eq. (13). Comparing $L_1 I_o^2/2$ with E_m shows that a maximum of ~81.5% of the matched load energy can be put into the storage inductor during the charging phase and this is achieved when $R_g\tau_p/L_1=1.25$. Second, from Eqs. (4a) and (7), the energy loss to switch heating is found to be $L_2 I_o^2/2$. This energy loss can be minimized by making L_2 as small as possible compared with L_1 as seen from the middle term in square brackets in Eq. (13). The remainder of the energy loss is associated with the term in the first square brackets in Eq. (13) and is due to energy being absorbed in the generator after the switch opens. This loss can be minimized by making R_ℓ large compared with R_g. Thus the energy

transfer efficiency is maximized when R_ℓ is large compared with R_g, when L_2 is small compared with L_1, and when L_1 is chosen such that $R_g\tau_p/L_1 \sim 1.25$.

This result should be contrasted with the special case of switching current from one inductor to another with no resistive elements in the circuit other than the switch. In this case $R_g = R_\ell = 0$ so that from Eq. (3) $\tau_+ = L_1L_2/[R_s(L_1+L_2)]$ and $\tau_- = 0$. The currents I_1 and I_2 then become $I_1 = [L_1I_o/(L_1+L_2)][1+(L_2/L_1)\exp(-t/\tau_+)]$ and $I_2 = [L_1I_o/(L_1+L_2)][1-\exp(-t/\tau_+)]$. The energy lost to switch heating is then $E_s = \int_0^\infty I_s^2 R_s dt = L_1L_2I_o^2/2(L_1+L_2)$ where $I_s = I_1 - I_2 = I_o \exp(-t/\tau_+)$. In the special case of $L_1 = L_2$ half of the stored energy, $E_o = L_1I_o^2/2$, is lost in the switch when it is opened. However, as long as $L_2 \ll L_1$, the switch loss is small (i.e. $E_s/E_o \sim L_2/L_1 \ll 1$).

The results of this lumped circuit analysis show that in order to obtain pulse compression and power multiplication with reasonable energy transfer requires $R_s \gg R_\ell \gg R_g$ and $L_2 \gg L_1$. The risetime of the load current is then τ_+ and the pulse width is $\sim\tau_-$ as given in Eq. (4). In a real system, however, the switch does not open instantaneously. If the switch opens in a time $\tau_{op} > 0$, then the switching time, τ_s, is given roughly by the larger of and τ_+. If $\tau_+ \ll \tau_{op}$, then the switch opening time is the dominant factor and $\tau_s = \tau_{op}$. Clearly τ_s must be small compared with the decay time of the load current, τ_-, or the power and energy to the load will be degraded. Thus the smallness of τ_s/τ_- is a figure of merit for the switch. When $\tau_s \approx \tau_{op} \gg \tau_+$, the expressions derived in Eqs. (11) and (13) overestimate M and E_ℓ/E_m respectively.

B. Transmission Line Analysis

In addition to finite opening time effects, finite transit time effects, which are not incorporated in a lumped circuit analysis, can also play an important role in defining system requirements and setting limits on the performance of the system. In particular these effects will become important when the switching time and output pulse duration become comparable with or shorter than the transit times of the elements in the transmission line. To study these effects let the storage inductor L_1 and the output inductor L_2 in Fig. 1 be replaced by transmission line elements with impedances Z_1 and Z_2, and electrical lengths $\tau_1=L_1/Z_1$ and $\tau_2=L_1/Z_1$ respectively. With the switch closed and the storage inductor current charged to I_o, a forward moving wave of voltage $V_+=I_o Z_1/2$ and backward moving wave of voltage $V_-=-I_o Z_1/2$ are superimposed on the line. The voltage at the switch $V_s=V_++V_-=0$ and the switch current $I_s=(V_+-V_-)/Z_1=I_o$. At this time the switch is opened.

First note that, if the switch opens on a timescale faster than the roundtrip transit time, $2\tau_1$, of the storage inductor, then the output pulse duration can be no shorter than $2\tau_1$. To illustrate this point consider the case where the switch opens instantaneously and at the same time the generator end of element one is shorted. The forward moving wave will be partially transmitted and partially reflected at the junction between elements one and two.[8] The transmission coefficient is $C_T=2Z_2/(Z_2+Z_1)$ and the reflective coefficient is $C_R=(Z_2-Z_1)/(Z_2+Z_1)$. The transmitted wave becomes a forward moving wave in element two with voltage $V_T=C_T V_+$ and corresponding current $I_T=V_T/Z_2$. Assuming for the moment that $Z_2=Z_1$, there will be no reflected wave at the junction between elements one and two. The original backward moving

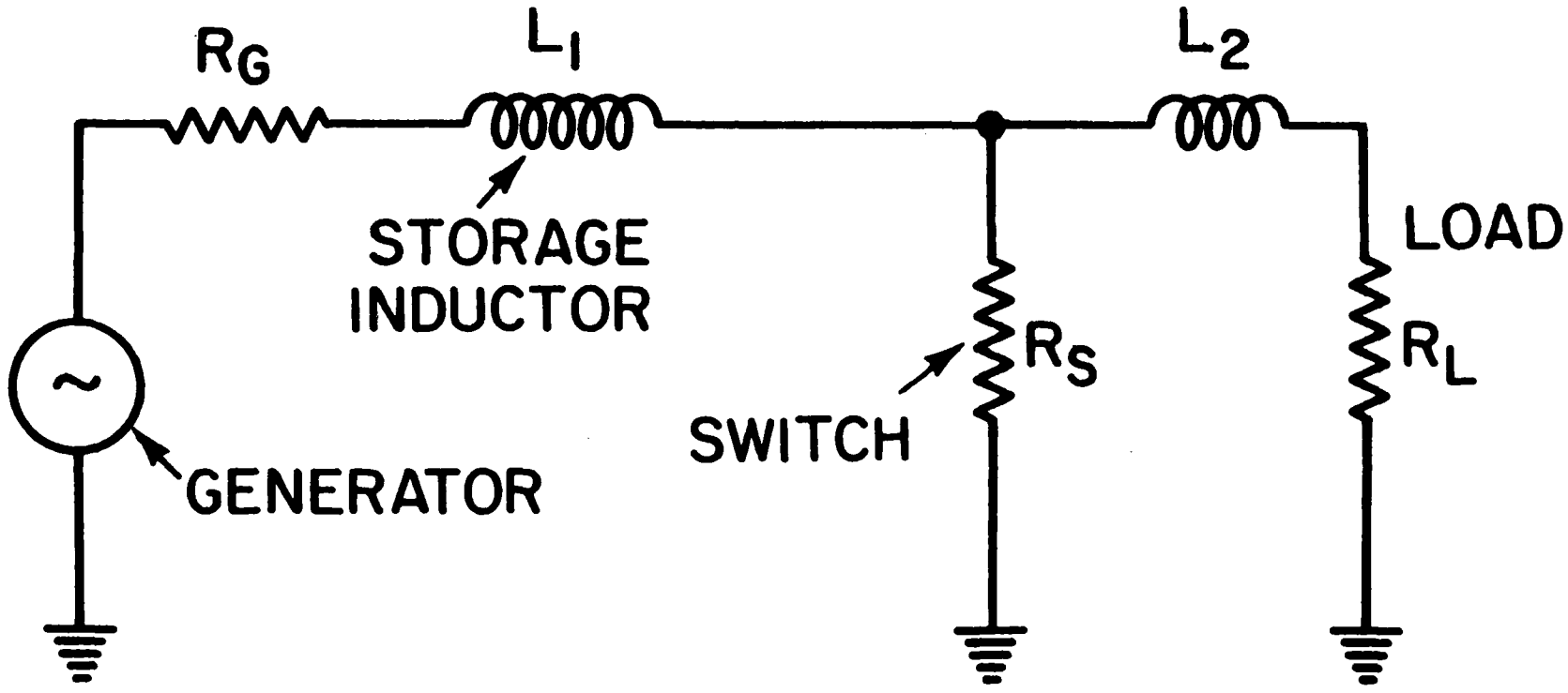

Figure 1 - Simple lumped circuit for analyzing system requirements for pulse compression and power multiplication using inductive storage techniques.

wave in element one simply inverts as it reflects off the shorted end at the generator side and moves forward immediately following the initial forward moving wave. The net result is a forward moving wave in element two of length $2\tau_1$. If $Z_2 \neq Z_1$, the pulse duration as measured by the envelope of the output voltage would be lengthened due to multiple reflections and the power, $P=I_T V_T$, would be reduced from the maximum value of $I_o^2 Z_1/4$ at $Z_2=Z_1$.

In order to prevent reflection at the load end of element two, the transmission line should be terminated with a matched load resistance $R_\ell=Z_2$. For $R_\ell=Z_2=Z_1$, all the energy stored in element one before the switch was opened will be delivered to the load resistor over a period $2\tau_1$, at a power level of $I_o^2 Z_1/4$. Thus for very fast switching times this is the minimum pulse width and maximum power that can be obtained. In terms of inductances this implies the system should be designed with $R_\ell=L_2/\tau_2=L_1/\tau_1$.

In summary the system requirements obtained from the simple lumped circuit analysis for optimum pulse compression and power multiplication using inductive storage are $L_1 \gg L_2$, and $R_s \gg R_\ell \gg R_g$. For short pulse operation transit time effects may become important requiring $R_\ell=L_2/\tau_2=L_1/\tau_1$ for optimum performance. In addition the switch requirements are threefold. First, the switch must be able to conduct large currents for the duration of the charging time, τ_p. Second, the switch should be able to change its resistance from $R_s \ll R_g$ to $R_s \gg R_\ell \gg R_g$. And finally this change must occur on a short timescale, namely $\tau_s \ll \text{Max}\{\tau_-, 2\tau_1\}$. The PEOS, which will now be discussed, has been shown to have these properties in a high power (~1TW) operating regime.[1]

III. PEOS Model

The PEOS, as used in recent experiments,[1] consists of a low density carbon plasma ($n_p \sim 10^{13} cm^{-3}$) injected through an anode screen of length towards the cathode of a coaxial vacuum transmission line. For the purposes of this model it is assumed that the plasma uniformly fills this annular region and that the conducting plasma provides a low resistance path for current flow. The plasma drifts towards the cathode with a velocity $v_d \sim 10^7 cm/s$. Also it is assumed that a high density plasma is formed on the cathode surface and provides an electron source. When a voltage is applied across the switch, a sheath is formed near the high density plasma on the cathode surface and the switch current is carried across this sheath in a bipolar space-charge-limited fashion.[9] The current flow in the plasma itself is not described here but will be treated in future work. The switch model describes the switch operation independent of treating plasma phenomena. It does assume, however, that the current flow in the plasma is predominantly radial so that radial $\underline{J} \times \underline{B}$ forces on the plasma are negligible.

The operation of the switch can be described by four phases: the conduction phase, the erosion phase, the enhanced erosion phase and the magnetic insulation phase. These phases, which are illustrated in Fig. 2, will now be described in detail. In what follows, unless specifically noted, currents will be in units of amperes with $e=1.6 \times 10^{-19}$ Coulombs, voltages will be in units of volts, resistances will be units of ohms and all other parameters will be in CGS units.

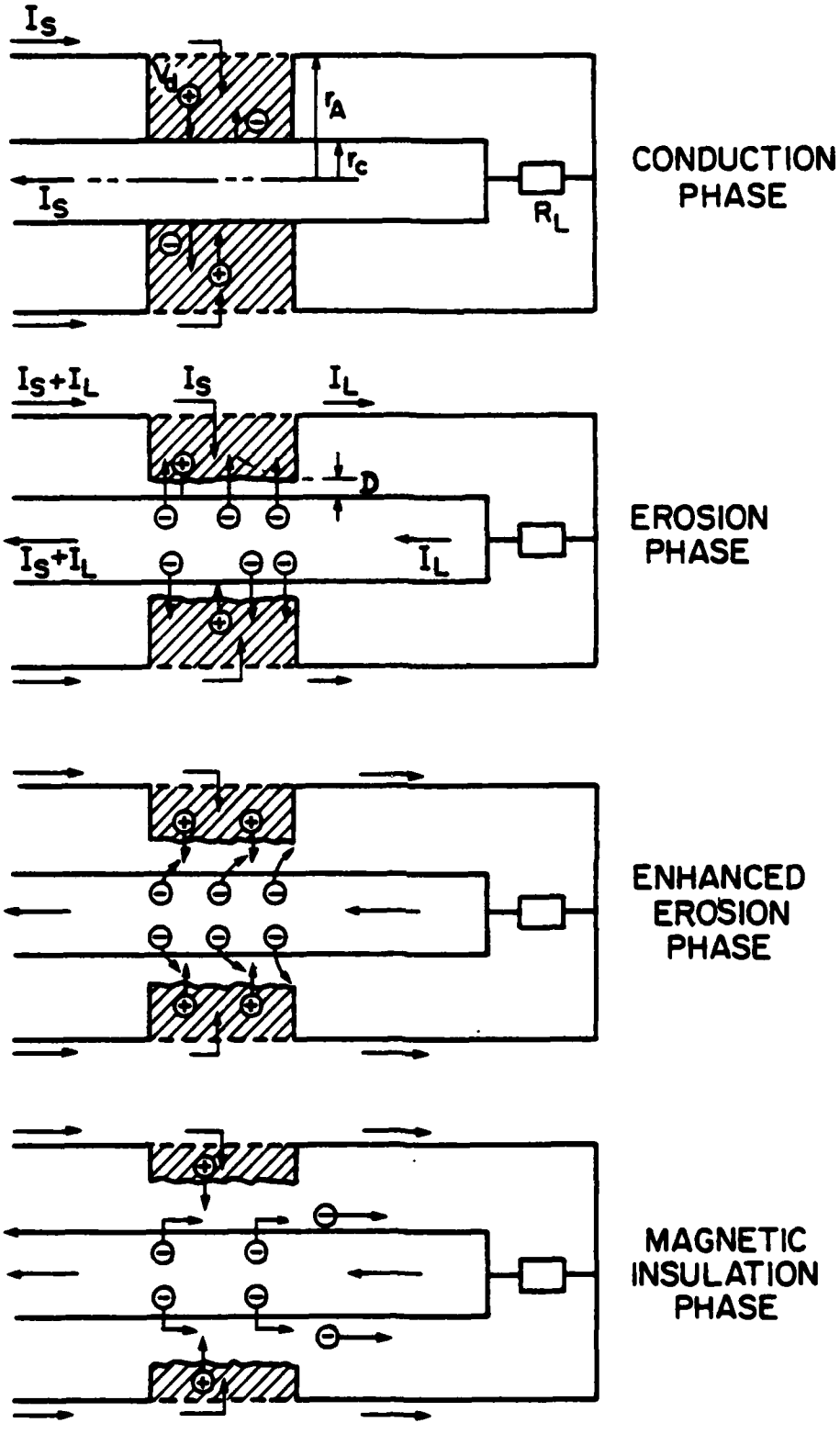

Figure 2 - Illustration of the different phase of PEOS operation showing the conduction phase, the erosion phase, the enhanced erosion phase and the magnetic insulation phase.

During the conduction phase ($R_s \sim 0$), ion current drawn from the switch plasma does not exceed the ion flux that the plasma drift is supplying to the cathode. This is illustrated in Fig. (2a). Here it is assumed that other sources of ion flux, such as ion temperature, are small compared with flux due to the plasma drift motion. Current is carried across the sheath at the cathode by both the ions (I_i) and electrons (I_e) in a bipolar space-charge-limited fashion, so that

$$\frac{I_i}{I_e} = \left(\frac{m_e Z}{m_p A}\right)^{\frac{1}{2}} \tag{14}$$

where Z and A are the charge state and atomic weight of the ions. For the C^{+2} plasma found in the switch[10], $I_i/I_e \sim .01$, so that the electrons carry most of the current, i.e. $I_e \sim I_s$. Thus, large switch currents can be carried before the ion current becomes comparable with the ion flux provided by the plasma drift. The conduction phase continues until

$$I_i \sim \left(\frac{m_e Z}{m_p A}\right)^{\frac{1}{2}} I_s > 2\pi \ell r_c n_p e Z v_d, \tag{15}$$

where r_c is the cathode radius and ℓ is the axial length of the plasma. Megampere level currents have been carried by the switch plasma in this fashion.[1]

Once the ion current begins to pull more ions off the plasma surface than the plasma drift can supply, the surface of the switch plasma begins to erode away and a gap forms. This is called the erosion phase and is illustrated in Fig. (2b). During this phase as the gap opens at a rate of $\gtrsim v_d$ and the switch resistance begins to increase but remains at a relatively small value ($<1\Omega$). The gap width D is determined by

$$dD/dt = I_i/2\pi\ell r_c n_p eZ - v_d \quad , \tag{16}$$

where I_i/I_e is given in Eq. (14),

$$I_e = 2.7 \times 10^{-5}\ \ell r_c V_s^{3/2}/D^2 \sim I_s \tag{17}$$

is the space-charge-limited current for bipolar flow with $D/r_c \ll 1$ and V_s, the voltage across the switch. This phase typically lasts a few nanoseconds and ends when the gap becomes larger than the electron Larmor radius that is, the magnetic field becomes strong enough to cause significant electron orbit bending in the gap. Simulations using particle-in-cell codes[11] for this geometry show that this occurs when the switch current I_s approaches the critical current I_c, so that

$$I_s \sim I_c \equiv 1.36 \times 10^4 (\gamma^2-1)^{\frac{1}{2}}\ r_c/D \quad , \tag{18}$$

where γ is the electron relativistic gamma factor which is related to V_s through $\gamma = 1 + 1.96 \times 10^{-6} V_s$.

The fast opening of the switch begins with the enhanced erosion phase when the gap opens rapidly due to ion current enhancement over that specified in Eq. (14) for one-dimensional bipolar flow. This enhanced erosion phase is illustrated in Fig. (2c). When the current exceeds the critical current as defined in Eq. (18) because the gap has opened enough for this geometry, the electron flow becomes two-dimensional and the electron space charge distribution is altered by the now large magnetic field. Electrons $\underline{E} \times \underline{B}$ drift axially in the self-consistent electric and magnetic fields in the gap, traveling a distance $\sim\ell$ instead of just crossing the gap, D, before being absorbed at the anode (i.e. the switch plasma). This new electron flow pattern increases the electron space charge near the plasma surface in a similar fashion as in an ion diode and thus greatly enhances the ion

current.[12] The enhanced ion current becomes

$$\frac{I_i}{I_e} \approx \left[\frac{2m_e Z(\gamma+1)}{m_p A}\right]^{\frac{1}{2}} \frac{\ell}{D} \quad . \tag{19}$$

This result is confirmed by numerical simulations for similar geometries.[11] Because the load current is still small at this time, electrons eventually cross the gap where the magnetic field falls off towards zero at the load end of the switch region.

For large initial ℓ/D, Eqs. (16) and (19) show that the gap opens rapidly under these conditions. Opening rates of $\sim 10^8$ cm/s are attainable. The total current in the switch region is limited to I_c. Larger currents are not allowed because the self-consistent magnetic field would prevent electrons from crossing the gap. The switch resistance is then $\sim V_s/I_c$ which increases with the rapidly increasing gap, D, as seen from Eq. (18). Since the large storage inductor holds the current nearly constant on this short timescale, the rising switch resistance also results in a rapid rise in the voltage across the switch and the load which is in parallel with the switch. This, in turn, results in the initiation of significant load current. The enhanced erosion phase typically lasts a few nanoseconds and ends when the load current becomes large enough to insulate the electron flow at the load end of the switch region.

The last phase of the switch operation is the magnetic insulation phase and is illustrated in Fig. (2d). As the load current increases and the electron flow at the load end of the switch region begins to be insulated, the electron current flowing across the gap in the switch region is limited to

$$I_e = I_c - I_\ell - I_i \quad , \tag{20}$$

where I_ℓ is the load current and now

$$I_i = 1.45 \times 10^{-5} \left(\frac{m_e Z}{m_p A}\right)^{\frac{1}{2}} \ell r_c V_s^{3/2}/D^2 \quad , \tag{21}$$

which is the one species space-charge-limited ion current. The ion current is no longer enhanced because of the bias current flowing down the inner conductor to the load which pulls the electrons away from the switch plasma. When $I_\ell \gtrsim I_c$, the electron flow is completely insulated so that $I_e=0$ and $I_s=I_i \ll I_c$. Electrons emitted from the cathode either return to the cathode or flow downstream to the load. The voltage across the switch is still large while the switch current has dropped dramatically so that the switch resistance has now reached a large value. Full insulation is typically achieved in a few nanoseconds after which the switch is considered open. Note that currents as large or larger than the critical current are required to open the switch in this fashion.

The model presented here predicts the voltage, current and impedance history of the PEOS as a function of the input waveforms, geometry and switch parameters. The switch remains closed during the conduction phase which can last for tens of nanoseconds. The switch opening commences with the erosion phase, accelerates during the enhanced erosion phase and is completed as the magnetic insulation phase begins. The entire opening phase lasts on the order of 10 ns. In the next section this model will be used with a simple open circuit voltage waveform to derive scaling laws for the switch operation. In Section V this model will be incorporated into a transmission line code in order to numerically model switch experiments.

IV. Scaling Laws

In order to design a PEOS for use on different pulsed power generators, scaling laws are necessary. To accomplish this a simple generalizing open circuit voltage waveform will be assumed where

$$V_{oc} = V_o \begin{cases} t/\tau_r, & 0 \leq t \leq \tau_r \\ 1, & \tau_r \leq t \leq \tau_p \\ 0, & t > \tau_p \end{cases} , \tag{22}$$

and where τ_r is the voltage risetime and V_o is the maximum voltage. The risetime in the voltage waveform gives a more realistic model for scaling purposes than the square waveform used in Section II. After some time τ_p the voltage will fall off to zero. It is assumed for the present inductive storage applications that $\tau_r < t_c < \tau_p$, where t_c is the conduction time of the switch. The conduction time is defined to be the time from t=0 until the ion current flowing in the switch exceeds the ion flux provided by the plasma drift.

During the conduction and erosion phases the switch resistance is small compared to the generator impedance so that to first order the switch acts like a short circuit and can be ignored in analyzing the circuit. The circuit equation then is simply

$$V_{oc} = R_g I_1 + L_1 \, dI_1/dt \tag{23}$$

where the notation is the same as in Fig. 1. Note that for simplicity an I dL/dt correction due to axial acceleration of the switch plasma has also been omitted. Solving Eqs. (22) and (23) with $I_1(0)=0$ yields

$$I_1 = \frac{V_o \tau_o}{R_g \tau_r}\left[\left(\frac{t}{\tau_o} - 1\right) + \exp\left(-\frac{t}{\tau_o}\right)\right], \quad 0 \le t \le \tau_r \quad , \tag{24a}$$

and

$$I_1 = \frac{V_o}{R_g}\left[1 + \frac{\tau_o}{\tau_r}\left(1-\exp\left[\frac{\tau_r}{\tau_o}\right]\right)\exp\left(-\frac{t}{\tau_o}\right)\right], \quad t \ge \tau_r \quad , \tag{24b}$$

where $\tau_o = L_1/R_g$. With $I_s = I_1$ and using Eqs. (15) and (24b), the conduction time is found to be

$$t_c = \tau_o \ell n\left[\frac{\frac{\tau_o}{\tau_r}\left(1-\exp\left[\frac{\tau_r}{\tau_o}\right]\right)}{\left(2\pi \ell r_c n_p e v_d R_g/V_o\right)\left(m_p AZ/m_e\right)^{\frac{1}{2}} - 1}\right] \quad . \tag{25a}$$

For $\tau_r/\tau_o < 1$ and $t_c/\tau_o < 1$, this expression can be expanded giving to first order

$$t_c \approx \frac{\tau_r}{2} + \left(2\pi \ell r_c n_p e v_d \tau_o R_g/V_o\right)\left(m_p AZ/m_e\right)^{\frac{1}{2}} \quad . \tag{25b}$$

Thus, t_c varies to first order in a linear fashion with n_p and thus can be tuned by varying the plasma density. For the typical parameters τ_r=25 ns, r_c=6 cm, r_a=12 cm, ℓ=5 cm, $n_p = 2 \times 10^{13}$ cm^{-3}, $v_d = 7.5 \times 10^6$ cm/s, τ_o=75 ns, R_g=2 Ω, V_o=3 MV, A=12 and Z=2, the conduction time is t_c=60 ns. These are representation of the parameters for the Gamble II experiments.[1]

After a time t_c, the gap, D, begins to open during the erosion phase. Combining Eqs. (15) and (16) and using $I_s = I_l$, from Eq. (24b) gives an equation for D(t) which can be integrated from t_c to t yielding

$$D(t) = \frac{\left[(t-t_c) - \frac{\tau_o}{\tau_r}\left(1-\exp\left[\frac{\tau_r}{\tau_o}\right]\right)\left(\exp\left[-\frac{t}{\tau_o}\right]-\exp\left[-\frac{t_c}{\tau_o}\right]\right)\right]}{(2\pi \ell r_c n_r e R_g/V_o)(m_p AZ/m_e)^{\frac{1}{2}}} - v_d(t-t_c). \tag{26a}$$

This equation can also be expanded to first order to give

$$D(t) \approx \frac{v_d(t-t_c)^2}{(2t_c-\tau_r)} \quad , \text{ for } t > t_c \quad , \tag{26b}$$

where Eq. (25b) was used to simplify the expression. To first order then D increases quadratically in time once the erosion phase begins. During the typical nanosecond timescale for the erosion phase the opening rate is on the order of 10^7cm/s. The opening rate during this phase is too slow to explain the experimentally observed fast switching action. Because the gap does not open very fast, the switch impedance and voltage also remain low during the erosion phase. Combining Eqs. (17) and (24b) shows that

$$V_s(t) = 1.1 \times 10^3 \left(\frac{V_o D^2(t)}{\ell r_c R_g}\right)^{2/3} \left[1 + \frac{\tau_o}{\tau_r}\left(1-\exp\left[\frac{\tau_r}{\tau_o}\right]\right)\exp - \frac{t}{\tau_o}\right]^{2/3} , \tag{27}$$

where one finds $V_s \ll V_o$ for the typical parameters listed previously and for D(t) given by Eq. (26b).

The erosion phase ends when the switch current exceeds the critical current. Thus, the duration of the erosion phase, t_e, can be obtained by equating Eqs. (24b) and (18) and substituting for D and V_s from Eqs. (26b) and (27) respectively. To first order this gives

$$t_e = \frac{3.75 \times 10^4 \, \tau_o r_c R_q / V_o}{\left[\ell v_d (t_c - \tau_r/2) \right]^{1/2}} \quad , \tag{28}$$

where $t_e \ll t_c - \tau_r/2$ was assumed in order to reduce the expression to this simple form. For the same parameters as used previously t_e = 8 ns, so that the critical current and ensuing enhanced erosion phase are quickly attained in this case. From Eqs. (25b) and (28) one finds that t_e scales as $n_p^{-1/4}$, thus varying the density to tune the conduction time does not greatly alter t_e.

The duration of the enhanced erosion phase can be obtained by solving Eqs. (16), (18) and (19) simultaneously. During this opening time it is assumed that 1) $I_s = I_c$, 2) $I_s \sim I_e \gg I_i$ even with the enhanced ion flow and 3) $I_s \sim I_{op}$=const. over this short time because of the large inductance L_1. In addition, the drift velocity term in Eq. (15) can be dropped because the enhanced erosion term dominates. The enhanced erosion time, t_n, is then given by

$$t_n = 1.1 \times 10^{-8} \, n_p (ZA)^{1/2} F(\gamma_p) \left(\frac{r_c}{I_{op}} \right)^3 \quad , \tag{29}$$

where $F(\gamma_p) = [(\gamma_p+1)^{3/2}/3 - 2^{3/2}/3 - (\gamma_p+1)^{1/2} + 2^{1/2}]$ and γ_p is the peak electron relativisitic gamma factor reached during the enhanced erosion phase. Note that t_n depends strongly on the magnetic field at the cathode ($B_c \sim I_{op}/r_c$) at

the time of opening. For the same parameters as used previously and with γ_p=10, and I_{op}=10^6 A, one finds t_n ~2.2 ns. The final gap can be obtained from Eq. (18) yielding $D(t_{op})$=0.8 cm, where t_{op}= t_c+ t_e+t_n.

Using t_e+ t_n as an estimate of the switching time is optimistic since it ignores any interaction with the load. In fact, the current begins to switch to the load as the switch begins to open. The electron flow is being pulled towards the cathode by the increasing magnetic field and eventually part of the electron flow becomes magnetically insulated at the load end of the switch and leaves the switch region to flow downstream to the load. This reduces the enhanced ion current from its peak value given in Eq. (19) and slows down the opening. A similar ion current reduction occurs in magnetically insulated ion diodes when the applied field is raised above the critical field. This process is further complicated if the load impedance varies in time as will be the case with electron- or ion-diode loads. For example, a high initial load impedance ($R_\ell \gtrsim R_s$ when the diode first turns-on) can last several nanoseconds and prevent rapid current switching until the diode impedance drops. Thus, the transition from the enhanced erosion phase to the magnetic insulation phase is not well defined. Similarly in a real system the distinction between opening time and switching time is unclear because of the interaction between the switch and load. Equation (29) then is only a guide for scaling purposes in designing opening switches. A computer code analysis of this complicated interaction is required to give a more accurate prediction of the switching time. This is done in the following section.

The important scaling for the conduction time, erosion time and opening time are then found in Eqs. (25), (28) and (29), respectively. These scaling laws give the insight necessary for designing switches for different regimes of operations. One final scaling law which should be considered concerns the axial acceleration of the plasma. Although radial $\underset{\sim}{J}\times\underset{\sim}{B}$ forces were not considered because the current in the plasma was assumed to be predominantly radial, axial $\underset{\sim}{J}\times\underset{\sim}{B}$ forces must be considered. The plasma should not be accelerated downstream out of the switch region before the switch opens. Assuming that the plasma does not compress and that the radial current density is uniform, the distance the plasma moves downstream before opening is just

$$Z_d = \frac{1.6 \times 10^{20} \tau_r^2 I_{op}^2 \ell n(r_a/r_c)}{A \ell n_p (r_a^2 - r_c^2)} G\left(\frac{t_c + t_e}{\tau_r}\right) , \qquad (30)$$

where $G(y)=(y^4-2y^3+1.5y^2-.4y)/(y-.5)^2$. Thus $z_d<\ell$ is required to hold the plasma in the switch region until opening occurs. For the parameters used in the previous examples $z_d/\ell \sim 0.4$. Since $G(y)\sim y^2$ for $y \gg 1$, Eq. (30) shows that for long conduction times the longer the switch remains closed (larger t_c+t_e), the lower the switch current must be at opening. Assuming that z_d/ℓ must be less than unity and that $t_c \gg \tau_r, t_e$, Eqs. (25b) and (30) show that

$$t_c I_{op} < \frac{2 \times 10^{-4} (A/Z)^{\frac{1}{2}} \ell (r_a^2 - r_c^2)}{r_c v_d \tau_o \ell n(r_a/r_c)} , \qquad (31)$$

where Eq. (10) with $R_g \tau_p / L_1 = 1.25$ was used to express V_o/R_g in terms of I_o. This result, which is independent of plasma density, clearly illustrates the trade off between going to longer conduction times and switching larger

currents. For the same parameters used in the example following Eq. (25b), this condition reduces to $t_c I_{op} < 0.11$. Since $t_c I_{op} \sim 0.064$ for that example, axial acceleration of the plasma was not significant, only moving the plasma a fraction of the switch length.

V. Numerical Modeling

A computer code was developed to model the switch operation in a realistic system. A transmission line code[13] framework was used to include transit time effects and models for the time-dependent switch and diode load impedances were developed. The transmission line elements were chosen to simulate the Gamble II experiments at the Naval Research Laboratory (NRL).

The diode impedance model was designed to exhibit the various aspects of the impedance time history observed in pinched beam diodes. At first the impedance is very large (i.e. an open circuit) until the voltage at the load reaches a critical turn-on value for a given anode-cathode gap in the diode. A turn-on condition of 0.4 MV/cm was used. After turn-on the diode current is ramped up from zero to the Child-Langmuir space-charge-limited current over a 8 ns period. The value of 8 ns is the typical turn-on time observed for pinch reflex diodes on Gamble II when $dE/dt \sim 10^{14}$ V/cm/s in the diode gap. The diode impedance is related to the diode current by $R_\ell = V/I$ where the space-charge-limited diode current is a specified function of voltage. Once the diode current reaches the critical current [defined similarly to Eq. (18)], the diode current is limited to this value because of self magnetic field effects. The diode impedance is then specified accordingly. The diode impedance model also accounts for gap closure by varying the gap, d, in time

according to $d=d_o-v_ct$ where d_o is the initial gap and v_c is the closure velocity. A typical closure velocity of 4×10^6 cm/s was used, so that after a time $t=d_o/v_c$ the diode impedance drops to zero. An initial gap of 0.6 cm and a cathode radius of 3.0 cm was used in all code runs reported here.

The impedance model for the switch is described in Section III with the switch impedance defined by $R_s=V_s/I_s$. During the conduction phase the switch is treated as a short circuit so that $V_s \sim R_s \sim 0$. During the erosion phase the impedance begins to rise. The switch voltage, V_s, is specified by the transmission line code and $I_s(V, D)$ is given by Eq. (17). The gap, D, is determined by integrating Eq. (16) where I_i is given by Eq. (14) for $I_s < I_c$ and by Eq. (19) for $I_s \sim I_c$. Once the critical current, I_c, is reached and the enhanced erosion begins the load current turns on and the switch current, $I_s=I_e+I_i$, is restricted by Eq. (20). For $I_s+I_\ell > I_c$ the electron current across the gap is completely magnetically cutoff and the ion current is reduced to the single species space-charge-limit current specified in Eq. (21). The transition in I_i from bipolar flow to enhanced flow to single species flow is modeled after the results found in Ref. 14.

A schematic of the transmission line circuit for the Gamble II inductive storage, PEOS experiment is shown in Fig. 3. The characteristic impedance, R_g, for the Gamble II generator is 2Ω. The open circuit voltage waveform which was used to drive this circuit was a fit to the experimentally determined waveform shown in Fig. 4. When the switch was kept closed for the entire pulse, the code shows the storage inductor charged up to a maximum current of ~0.87 MA. With no switch in the circuit the code shows a maximum diode load current of 0.4 MA.

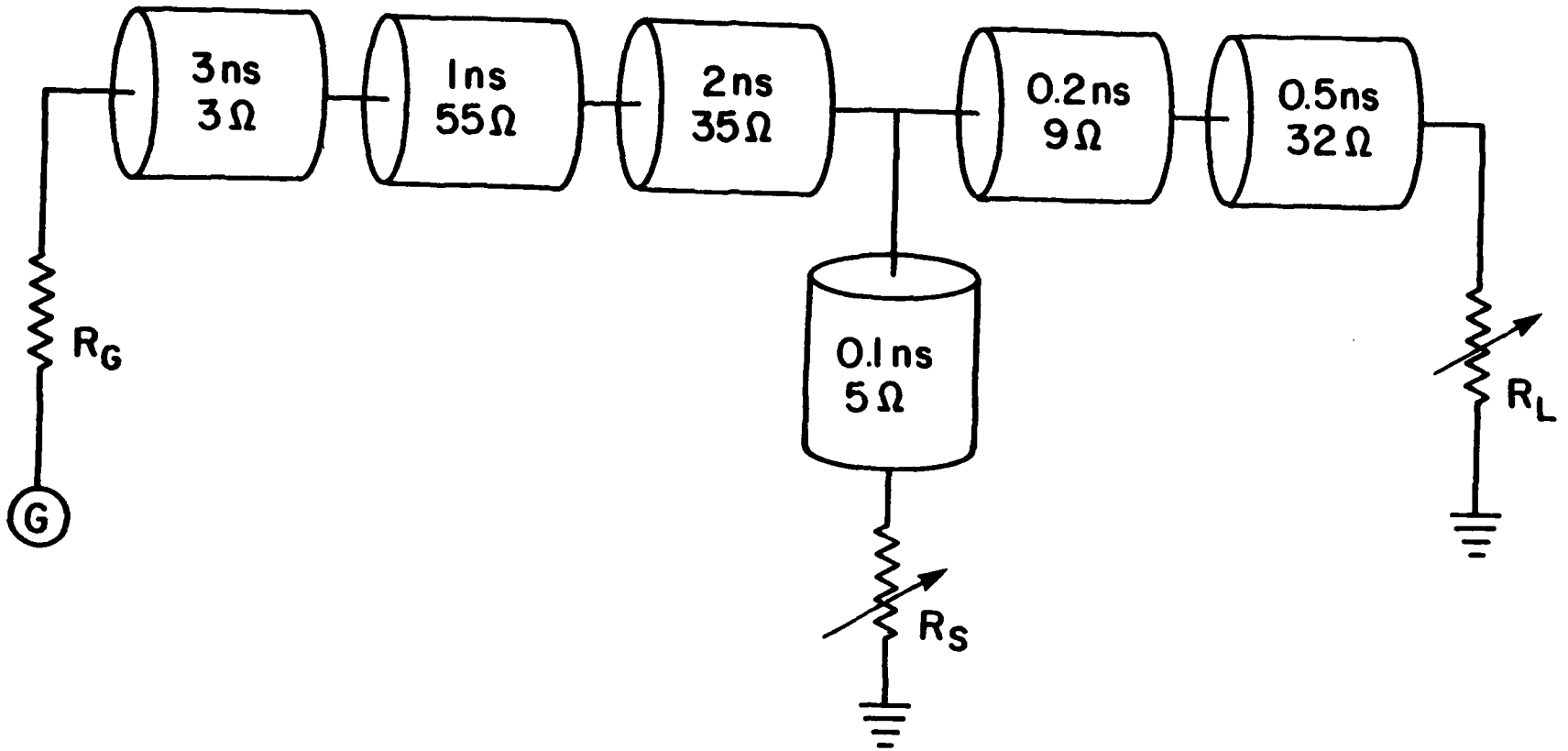

Figure 3 - Equivalent transmission line circuit for Gamble II PEOS experiment. The characteristic length and impedance of each element is shown.

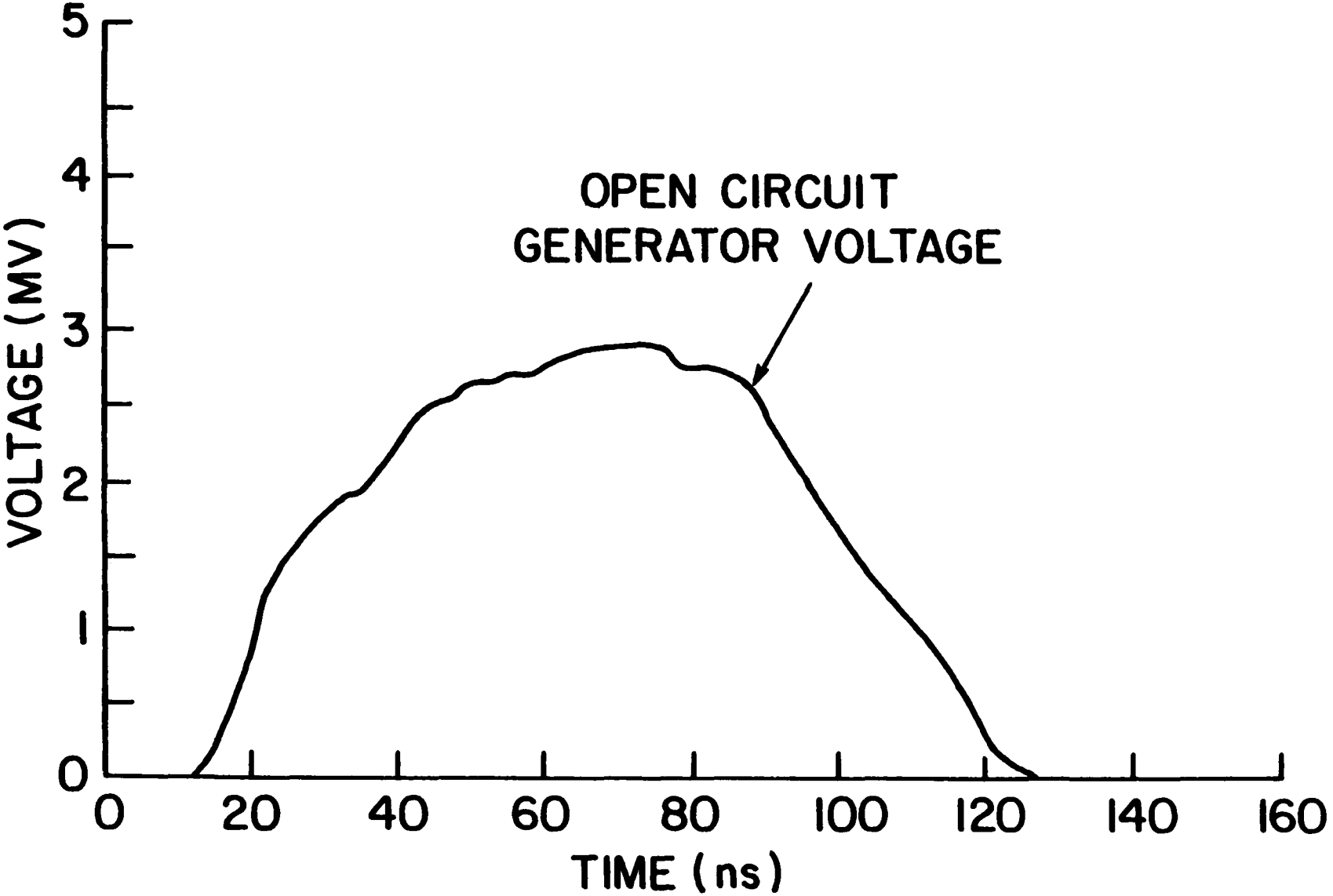

Figure 4 - Open circuit generator voltage waveform for Gamble II at 35 kV charging voltage.

The switch plasma parameters were chosen to be Z=1, A=12, v_d=7.5x10^{6}cm/s, ℓ=5.7 cm, r_c=6.35 cm and r_a=11.4 cm and n_p was varied. Figures 5, 6 and 7 show results from code runs where the plasma density was set at 1x10^{13}cm^{-3}, 1.5x10^{13}cm^{-3} and 2x10^{13}cm^{-3} respectively. First note that changing n_p by a factor of two changes the conduction time from ~37ns to ~72ns. Assuming that τ_r~25ns, τ_o=75ns, R_g=2Ω and V_o=3MV, the estimates of ~36ns and ~71ns from Eq. (25a) for the same two conduction times are in good agreement.

The results in Fig. 7 show switch opening close to the time of peak current in the storage inductor. The switching time is ~12 ns which, as expected, is longer than the estimate t_e+t_n~9 ns from the analytic model. The results displayed in Fig. 7 show a pulse compression of ~2.9, a voltage multiplication of ~2.5 and a power multiplication of ~1.6 compared with that obtained with a matched load. Assuming that R_s~20Ω and R_ℓ~7.5 at peak power and that L_1~150nH, L_2~20nH and τ_p ~75ns full-width-half-maximum, then the lumped circuit analysis of Section II predicts a pulse compression of τ_p/τ_-~4.7, a voltage multiplication of $(MR_\ell/R_g)^{1/2}$~3.0 and a power multiplication of M~2.4. As expected, these estimates are too high by ~50% because of the simplifying assumptions of instantaneous opening and constant load impedance. For the case studied here transit time effects are insignificiant.

This transmission line code analysis which incorporates both the switch impedance model described in Section III and a diode load impedance model should be capable of accurately modeling experimental conditions. In the following section results from this code will be used to compare with actual experimental data.

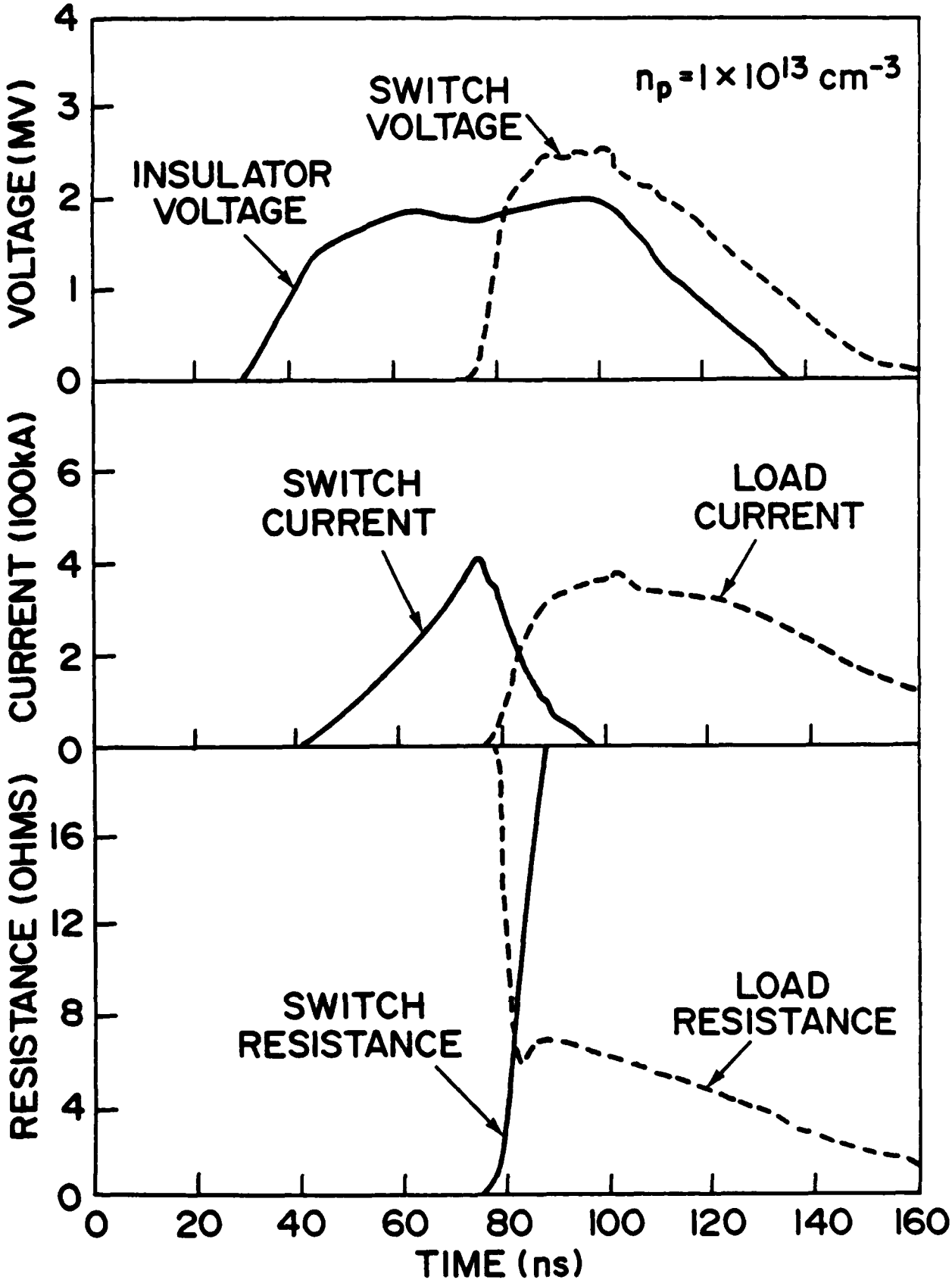

Figure 5 - Code results with $n_p = 1 \times 10^{13}$ cm^{-3}.

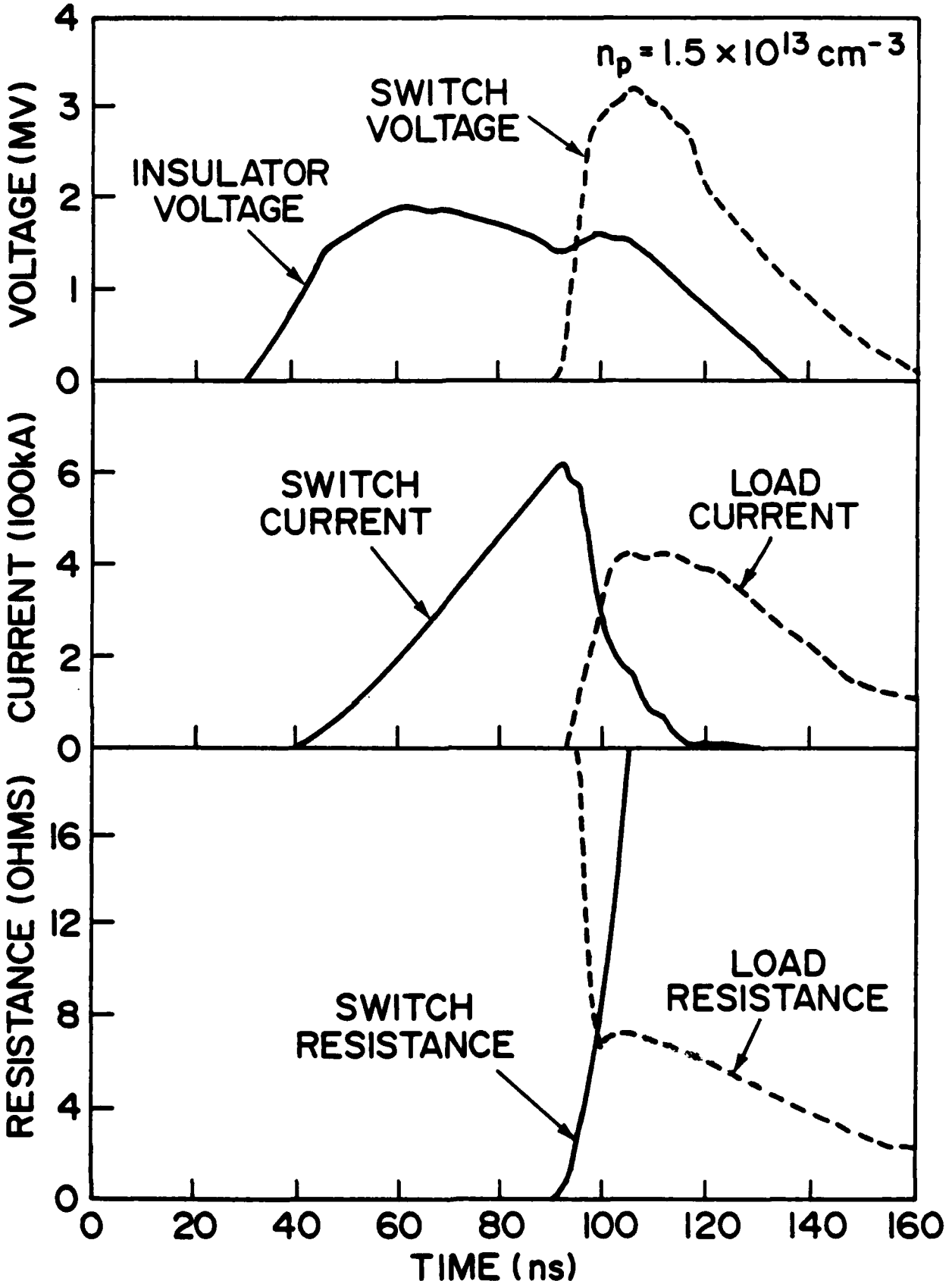

Figure 6 - Code results with $n_p = 1.5 \times 10^{13}\ cm^{-3}$.

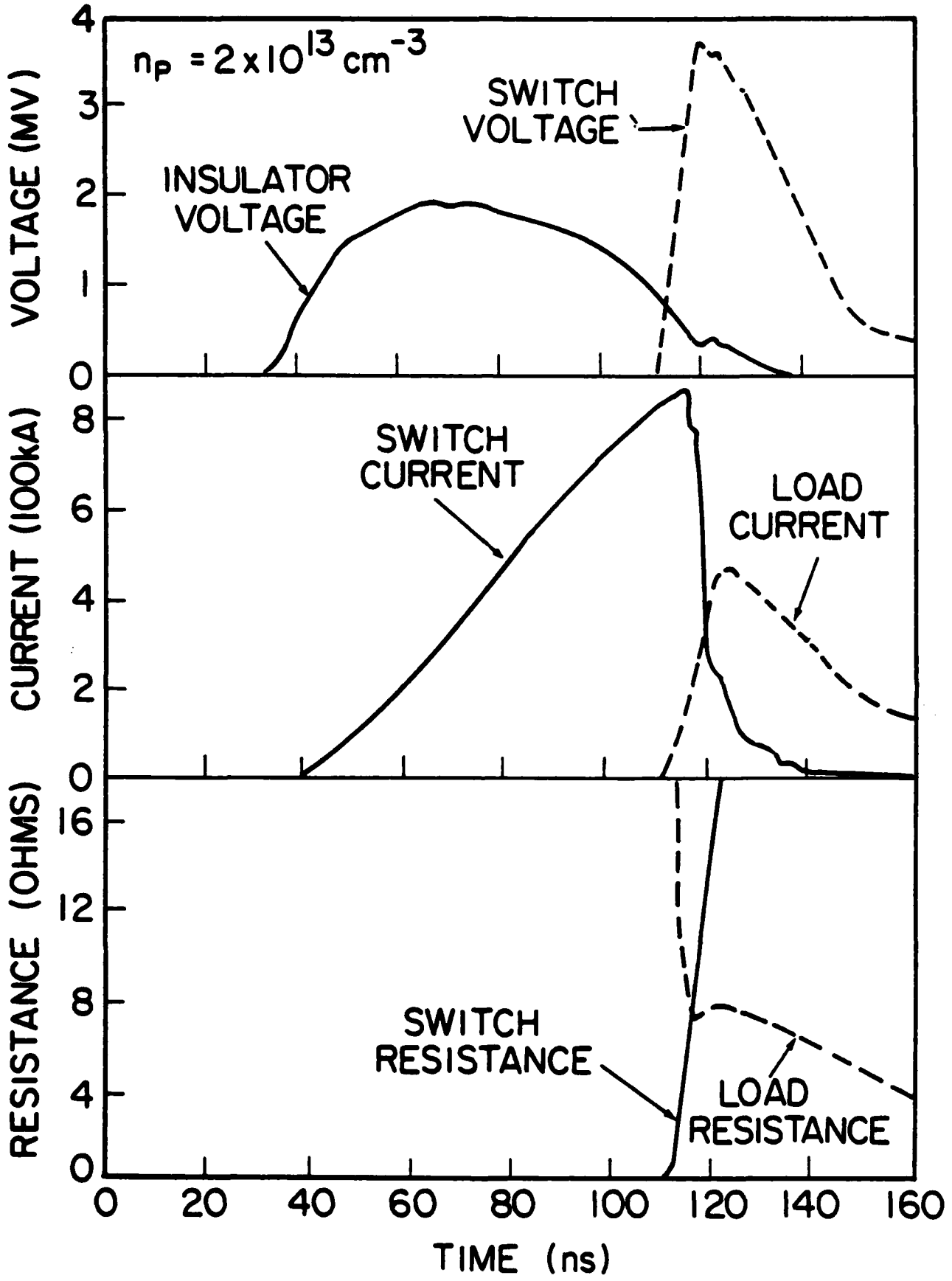

Figure 7 - Code results with $n_p = 2 \times 10^{13}\ cm^{-3}$.

VI. Experimental Comparison

Experimental results from a Gamble II shot are shown in Fig. 8. This shot was chosen because it clearly illustrates many of the physics issues being studied. The insulator voltage is measured on the load side of R_g and the switch voltage is just the insulator voltage corrected for LdI/dt where L is the inductance between the insulator and the switch. The foot on the switch voltage from 70 to 90 ns results from not including an IdL/dt correction due to the axial acceleration of the switch plasma. Estimates of this correction from Eq. (30) agree well with the magnitude of the correction seen in Fig. 8. Experimentally the storage inductor current and the load current are measured so that the switch current as shown in Fig. 8 is the difference of these two currents. The switch and load resistances are calculated from V/I where the load voltage results from a inductive correction to the switch voltage.

Even though the switch opened before the storage inductor was fully current charged, the results show a voltage pulse compression of ~2.7, a voltage multiplication of ~2.1 and a power multiplication of ~1.1 at the load compared with what one would expect with a matched load shot. For a fully current charged storage inductor the simple lumped circuit analysis of Section II predicts a pulse compression of $\tau_p/\tau_- \sim 5.5$ for $L_1 \sim 135$ nH and $R_\ell \sim 8\Omega$, voltage multiplication of $(MR_\ell/R_g)^{1/2} \sim 3.9$ and a power multiplication of $M \sim 3.8$ for $L_2 \sim 18$ nH and $R_s \sim 20\Omega$ at peak power. The pulse compression and voltage multiplication estimates are about a factor of two higher than the experimental results and the power multiplication estimate is even higher than those observed. There are three reasons for these differences.

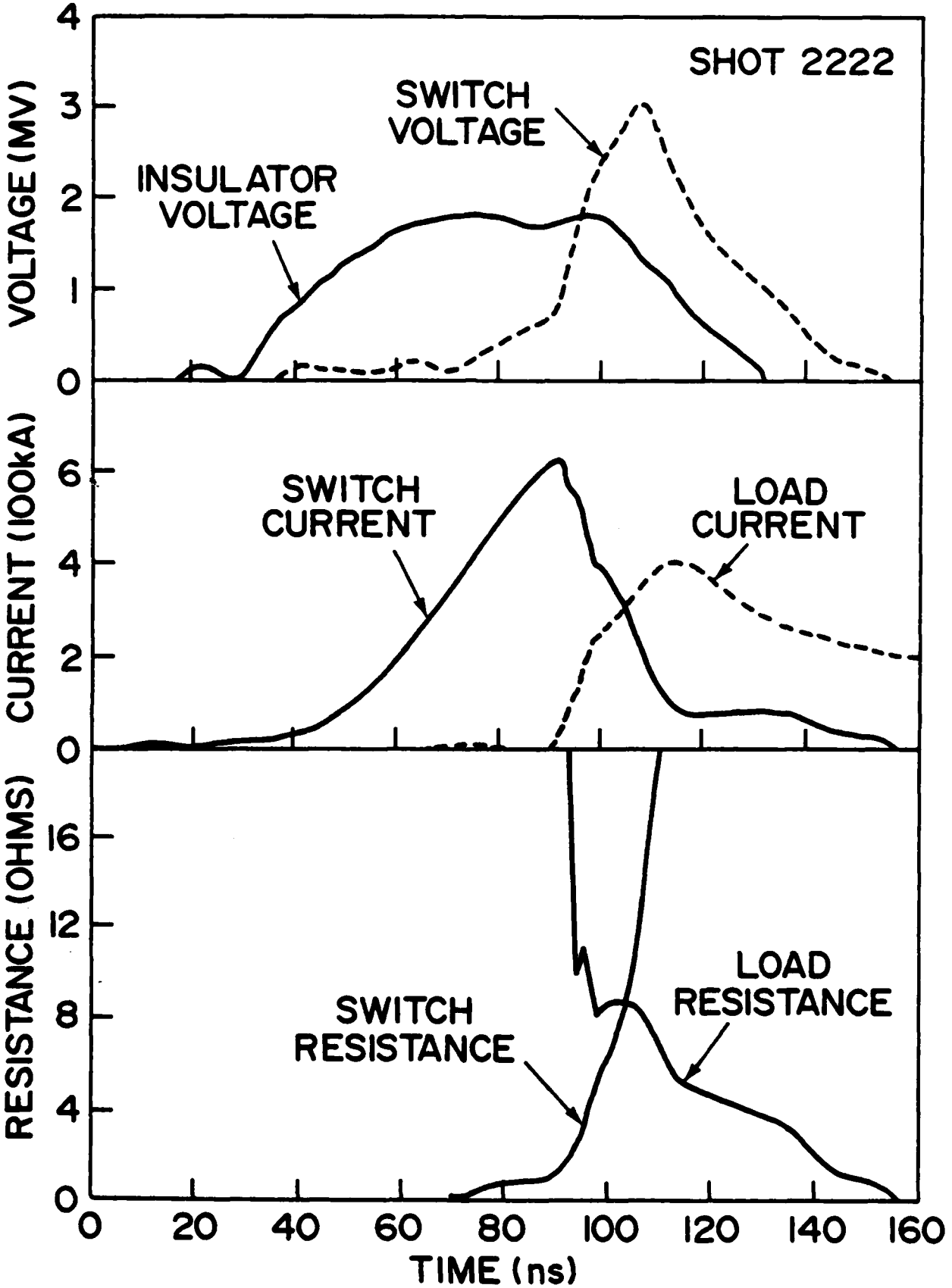

Figure 8 - Experimental data from a typical Gamble II shot.

First, the switch was opened early (at ~0.63 MA) before the inductor was fully charged (i.e. 0.87 MA) and while the generator was still driving the circuit. Since the power scales as I^2, this represents a factor of 2 decrease in power. Second, the opening time of the switch is not instantaneous as evidenced by the ~15 ns risetime of the switch resistance shown in Fig. 8. The switching time was thus determined by this opening time rather than the faster $\tau_+ = L_2/R_s$ ~1 ns timescale. Since the switching time was comparable with the decay time of the output pulse τ_- ~13.5 ns, the maximum voltage and power delivered to the load was limited as discussed in Section II. And thirdly, a significant fraction of the load current is diverted across the vacuum feed betweeen the switch and the diode. The magnetically insulated vacuum electron flow is apparently disrupted after ~7 ns as evidenced by the sharp change in the slope of the load current at ~100 ns and damage on the anode side of this vacuum section. This degrades the power multiplication factor since it reduces the load current just when the voltage is peaking. This lost load current appears as switch current in Fig. 8 because of the way the switch current is calculated. A computer code anlysis is required to model this early opening situation as well as the complicated interaction between the switch and load which determines the switching time.

The transmission line code was run to try to more closely model the experimental results. Since the axial acceleration of the plasma is not included in the code and the magnetically insulated flow is assumed stable, the IdL/dt foot on the switch voltage and the lost load current will not appear in the numerical results. The plasma parameters Z=1, A=12, $v_d = 7.5 \times 10^6$ cm/s, $\ell = 5.7$ cm, $r_c = 6.35$ cm and $r_a = 11.4$ cm were chosen to match the experimental parameters and n_p was varied to find a fit to the data given

in Fig. 8. The case with $n_p = 1.5 \times 10^{13} cm^{-3}$ in Fig. 6 most closely fits the experimental data in Fig. 8 with the current beginning to switch at the same time in both cases.

The numerical results in Fig. 6 show a peak switch voltage of ~3.3 MV at ~106 ns compared with ~3.0 MV at ~108 ns for the experimental results. The full-width-half-maximum voltage pulse width of ~34 ns for the code results is somewhat larger than the voltage pulse width of ~28 ns for the experimental results. The initial slope of the rising load currents agree very closely but after ~7 ns the slope abruptly changes in the experimental results. Consequently the peak load current observed experimentally occurs later at a lower voltage and is slightly smaller than that obtained in the numerical results. This is due to partial loss of the magnetically insulated electron flow between the switch and the load. The same ~15 ns switching time is observed in both Fig. 6 and Fig. 8.

The code results, which properly account for the interaction between the time varying switch and load impedances are in much better agreement with the experimental data than the simple lumped circuit analysis presented earlier. The numerical results in Fig. 6 give good qualitative agreement and reasonable quantitative agreement with the data in Fig. 8. The results shown in Figs. 5 and 7 indicate how the conduction time can be tuned by simply varying the plasma density.

VII. Summary

The simple lumped circuit analysis and the transmission line analysis of Section II provide insight into the requirements for designing an inductive storage system for pulse compression and power multiplication. It was found that $L_1 \gg L_2$ and $R_s \gg R_\ell \gg R_g$ is required as well as $R_\ell \sim L_2/\tau_2 \sim L_1/\tau_1$. In particular, $R_\ell > R_g$ is required for pulse compression with the output pulse width limited to a minimum of $2\tau_1$. Estimates of pulse compression and power multiplication were only within a factor of 2 of the experimentally observed values because this analysis assumed that the switch opened instantaneously and that the load had a constant resistance in time. The numerical modeling found in Sections V and VI, however, does properly include the time dependence of the switch and load impedances as well as transit time effects which are important in certain applications. The code results give good qualitative agreement as well as reasonable quantitative agreement with experimental results.

The switch impedance model used in this code is based on the physics understanding of how the switch operates as discussed in Section IV. The switch goes through four phases. The conduction phase lasts tens of nanoseconds and ends when the ion current drawn across the switch gap exceeds the plasma flux providing ions to the surface of the switch plasma. The erosion phase, which then commences, typically lasts for a few nanoseconds as the surface of the switch begins to erode away. Once the current exceeds the critical current, the enhanced erosion phase begins and provides the fast gap opening required for pulse compression and power multiplication. The mechanism responsible for fast gap opening in this model is the enhancement of the ion current due to redistribution of the electron space charge in the

presence of strong magnetic fields, similar to the phenomena observed in pinch beam diodes. This phase typically lasts on the order of a couple of nanoseconds and is followed by the magnetic insulation phase. Here the electron flow at the load end of the switch region becomes magnetically insulated as the current switches to the load. Scaling laws for estimating these timescales were derived in Section IV. Of particular importance is the scaling for the conduction time which was found to vary approximately linearly with density. The actual switching time, however, involves a complicated interaction between the switch and the load and requires the transmission line code analysis for an accurate estimate.

This work provides a basic understanding of PEOS operation, however, there are still many questions left unanswered. For example, the physics of the current flow in the plasma was not treated. Future work will include this and, in particular, will study two-dimensional effects such as the current distribution in the plasma. The resulting JXB forces on the plasma can affect gap opening as well as cause the gap to open differently along the axis. Understanding the mechanisms controlling the loss of magnetically insulated flow between the switch and the load will also be pursued so that this current loss can be minimized or even eliminated. Finally, the code developed here will be used as a guide in designing new experiments using the PEOS.

ACKNOWLEDGMENTS

The authors would like to acknowledge useful discussions with R. Kulsrud, G. Cooperstein, R.J. Commisso, D. Hinshelwood, S.W. McDonald, J.M. Neri and B.V. Weber.

This work was supported in part by the U.S. Department of Energy and by the Defense Nuclear Agency.

REFERENCES

1. R.A. Meger, R.J. Commisso, G. Cooperstein, Shyke A. Goldstein, Appl. Phys. Lett. 42, 943 (1983); R.A. Meger, J.R. Boller, D. Colombant, R.J. Commisso , G. Cooperstein, Shyke A. Goldstein , R. Kulsrud , J.M. Neri , W. F. Oliphant, P.F. Ottinger , T.J. Renk , J.D. Shipman, Jr. , S.J. Stephanakis, F.C. Young, and B.V.Weber , in Proc. of the 4th International IEEE Pulsed Power Conf. (Albuquerque, NM, June 1983).

2. C.W. Mendel, Jr., and S. A. Goldstein, J. Appl. Phys 48, 1004 (1977); P.A. Miller, J.W. Poukey and T.P. Wright, Phys. Rev. Lett. 35, 940 (1975).

3. R. A. Meger and F. C. Young, J. Appl Phys. 53 8543 (1982).

4. R.J. Commisso, R.F. Fernsler, V.E. Sherrer, and I.M. Vitkovitsky, in Proc. of the 4th International IEEE Pulsed Power Conf. (Albuquerque, NM, June 1983).

5. P.J. Turchi, in Proc. of the 4th International IEEE Pulsed Power Conf. (Albuquerque, NM, June 1983).

6. F. Venneri, J. Mandrekas, G. Gerdin, in Proc. of the 4th International IEEE Pulsed Power Conf. (Albuquerque, NM, June 1983).

7. B. Ecker, in the Proc. of the 4th International IEEE Pulsed Power Conf. (Albuquerque, NM , June 1983); S. Humphries and X. Fu, J. Appl. Phys. 54, 4629 (1983).

8. W. C. Johnson, "Transmission Lines and Networks," (McGraw-Hill, New York, 1950).

9. I. Langmiur and K.B. Blodgett, Phys. Rev. Series 2, 22, 347 (1923); I. Langmiur, Phys. Rev. Series 2, 2, 450 (1913).

10. J.M. Neri, R.J. Commisso, Shyke A. Goldstein, R.A. Meger, P.F. Ottinger, B.V. Weber and F.C. Young, 1983 IEEE Conf. on Plasma Sci., Conference Record - Abstracts (San Diego, CA, May 23-25, 1983), p. 124.

11. R.J. Barker and S.A. Goldstein, Bull. Am. Phys. Soc. 26, 921 (1981).

12. S.A. Goldstein and R. Lee, Phys. Rev. Lett. 35, 1079 (1975).

13. D. Hinshelwood, Naval Research Laboratory Memorandum Report 5185 (1983).

14. K. D. Bergeron, Appl. Phys. Lett. 28, 306 (1976).

DISTRIBUTION LIST

Director
Defense Nuclear Agency
Washington, DC 20305
Attn: TISI Archieves 1 copy
TITL Tech. LIbrary 3 copy
J. Z. Farber (RAEV) 1 copy
H. Soo (RAEV) 1 copy
J. Benson (RAEV) 1 copy

U.S. Department of Energy
Division of Inertial Fusion
Washington, DC 20545
Attn: L. E. Killion 1 copy
S.L. Kahalas 1 copy
R.L. Schriever 1 copy

U.S. Department of Energy
Office of Classification
Washington, DC 20545
Attn: Robert T. Duff 1 copy

U.S. Department of Energy
Nevada Operations Office
Post Office Box 14100
Las Vegas, NV 89114
Attn: Rex Purcell 2 copies

U.S. Department of Energy
P.O. Box 62
Oak Ridge, TN 37830 2 copy

Air Force Office of Scientific Research
Physics Directorate
Bolling AFB, DC 20332
Attn: A. K. Hyder 1 copy
M. A. Stroscio 1 copy

Air Force Weapons Laboratory, AFSC
Kirtland AFB, NM 87117
Attn: NTYP (W. L. Baker) 1 copy

Atomic Weapons Research Establishment
Building H36
Aldermaston, Reading RG 7 4PR
United Kingdom
Attn: J.C. Martin 1 copy

Boeing Company, The
P.O. Box 3707
Seattle, WA 98124
Attn: Aerospace Library 1 copy

Brookhaven National Laboratory
Upton, NY 11973
Attn: A.F. Maschke 1 copy

BMO/EN
Norton AFB, CA
Attn: ENSN 1 copy

Commander
Harry Diamond Laboratory
2800 Powder Mill Rd.
Adelphi, MD 20783
(CNWDI-INNER ENVELOPE: ATTN: DELHD-RBH)
Attn: DELHD-NP 1 copy
DELHD-RCC -J.A. Rosando 1 copy
DRXDO-RBH - K. Kerris 1 copy
DRXDO-TI - Tech Lib. 1 copy

Cornell University
Ithaca, NY 14850
Attn: D.A. Hammer 1 copy
R.N. Sudan 1 copy

Defense Advanced Research Project Agency
1400 Wilson Blvd.
Arlington, VA 22209
Attn: R. L. Gullickson 1 copy

Defense Technical Information Center
Cameron Station
5010 Duke Street
Alexandria, VA 22314
Attn: T.C. 2 copies

JAYCOR, Inc.
205 S. Whiting Street
Alexandria, VA 22304
Attn: J. Guillory 1 copy

Kaman Tempo
816 State Street (P.O. Drawer QQ)
Santa Barbara, CA 93102
Attn: DASIAC 1 copy

KMS Fusion, Inc.
3941 Research Park Drive
P.O. Box 1567
Ann Arbor, MI 48106
Attn: Alexander A. Glass 1 copy

Lawrence Berkeley Laboratory
Berkeley, CA 94720
Attn: D. Keefe 1 copy

Lawrence Livermore National Laboratory
P.O. Box 808
Livermore, CA 94550
Attn:
Tech. Info. Dept. L-3 1 copy
D.J. Meeker 1 copy
R.E. Batzel/J. Kahn,L-1 1 copy
J.L. Emmett, L-488 1 copy
J.F. Holzrichter, L-481 1 copy
W.F. Krupke, L-488 1 copy
J.H. Nuckolls, L-477 1 copy

Los Alamos National Laboratory
P.O. Box 1663
Los Alamos, NM 87545
Attn: M. Gillispie/Theo.Div. 1 copy
S.D. Rockwood,ICF Prog. Mgr.
DAD/IF M/S 527 6 copies

Massachusetts Institute of Technology
Cambridge, MA 02139
Attn: R.C. Davidson 1 copy
G. Bekefi 1 copy

Maxwell Laboratories, Inc.
9244 Balboa Avenue
San Diego, CA 92123
Attn: J.Pearlman 1 copy

Mission Research Corporation
1400 San Mateo Blvd. SE
Albuquerque, NM 87108
Attn: B.B. Godfrey 1 copy

National Science Foundation
Mail Stop 19
Washington, DC 20550
Attn: D. Berley 1 copy

Naval Research Laboratory
Addressee: Attn: Name/Code
Code 2628 -TID Distribution 20 copies
Code 4000 - T. Coffey 1 copy
Code 4040 - J. Boris 1 copy
Code 4700 - S.L. Ossakow 26 copies
Code 4704 - C. Kapetanakos 1 copy
Code 4720 - J. Davis 1 copy
Code 4730 - S. Bodner 1 copy
Code 4740 - V. Granatstein 1 copy
Code 4760 - B. Robson 1 copy
Code 4770 - I.M. Vitkovitsky 10 copies
Code 4771 - F. C. Young 1 copy
Code 4773 - G. Cooperstein 10 copies
Code 4773 - S.J. Stephanakis 1 copy
Code 4790 - D. Colombant 1 copy
Code 4790 - I. Haber 1 copy
Code 4790 - M. Lampe 1 copy
Code 6682 - D. Nagel 1 copy
Code 4773 - P. Ottinger 100 copies

Office of Naval Research
London Branch Office
Box 39
FPO New York, NY 09510
Attn: Dr. David Mosher 1 copy

Physics International Co.
2700 Merced Street
San Leandro, CA 94577
Attn: A.J. Toepfer 1 copy

Pulse Sciences, Inc.
1615 Broadway, Suite 610
Oakland, CA 94612
Attn: S. Putnam 1 copy

R&D Associates
Suite 500
1401 Wilson Blvd.
Arlington, VA 22209
Attn: P.J. Turchi 1 copy

R&D Associates
P.O. Box 9695
Marina Del Ray, CA 90291
Attn: C. MacDonald 1 copy

Sandia National Laboratories
P.O. Box 5800
Albuquerque, NM 87185
Attn: P.Vandevender / 1260 6 copies

Spire Corporation
P.O. Box D
Bedford, MA 01730
Attn: R.G. Little 1 copy
Stanford University
SLAC
P.O. Box 4349

Stanford, CA 94305
Attn: W.B. Herrmannsfeldt 1 copy

University of California
Irvine, CA 92717
Attn: N. Rostoker 1 copy

University of Rochester
250 East River Road
Rochester, NY 14623
Attn: J. Eastman 1 copy

Univ. of Washington
Dept. of Nuclear Engineering
BF-10
Seattle, WA 98115
Attn: F. Ribe 1 copy

Figure 7 - Code results with n_p=2x10$^{}$ cm$^{}$.